Article

Design of a Portable Analyzer to Determine the Net Exchange of CO$_2$ in Rice Field Ecosystems

Mirko Bonilla-Cordova [1], Lena Cruz-Villacorta [2], Ida Echegaray-Cabrera [1], Lia Ramos-Fernández [3,*]
and Lisveth Flores del Pino [4]

[1] Department of Environmental Engineering, Universidad Nacional Agraria La Molina, Lima 15024, Peru; 20170330@lamolina.edu.pe (M.B.-C.); 20170031@lamolina.edu.pe (I.E.-C.)

[2] Department of Territorial Planning and Doctoral Program of Engineering and Environmental Sciences, Universidad Nacional Agraria La Molina, Lima 15024, Peru; lenacruz@lamolina.edu.pe

[3] Department of Water Resources, Universidad Nacional Agraria La Molina, Lima 15024, Peru

[4] Research Center for Environmental Chemistry, Toxicology and Biotechnology, Universidad Nacional Agraria La Molina, Lima 15024, Peru; lisveth@lamolina.edu.pe

* Correspondence: liarf@lamolina.edu.pe

Abstract: Global warming is influenced by an increase in greenhouse gas (GHG) concentration in the atmosphere. Consequently, Net Ecosystem Exchange (NEE) is the main factor that influences the exchange of carbon (C) between the atmosphere and the soil. As a result, agricultural ecosystems are a potential carbon dioxide (CO$_2$) sink, particularly rice paddies (*Oryza sativa*). Therefore, a static chamber with a portable CO$_2$ analyzer was designed and implemented for three rice plots to monitor CO$_2$ emissions. Furthermore, a weather station was installed to record meteorological variables. The vegetative, reproductive, and maturation phases of the crop lasted 95, 35, and 42 days post-sowing (DPS), respectively. In total, the crop lasted 172 DPS. Diurnal NEE had the highest CO$_2$ absorption capacity at 10:00 a.m. for the tillering stage (82 and 89 DPS), floral primordium (102 DPS), panicle initiation (111 DPS), and flowering (126 DPS). On the other hand, the maximum CO$_2$ emission at 82, 111, and 126 DPS occurred at 6:00 p.m. At 89 and 102 DPS, it occurred at 4:00 and 6:00 a.m., respectively. NEE in the vegetative stage was -25 μmolCO2 m^2 s^{-1}, and in the reproductive stage, it was -35 μmolCO2 m^2 s^{-1}, indicating the highest absorption capacity of the plots. The seasonal dynamics of NEE were mainly controlled by the air temperature inside the chamber (Tc) (R = -0.69), the relative humidity inside the chamber (RHc) (R = -0.66), and net radiation (R$_n$) (R = -0.75). These results are similar to previous studies obtained via chromatographic analysis and eddy covariance (EC), which suggests that the portable analyzer could be an alternative for CO$_2$ monitoring.

Keywords: sensors; infrared detectors; camera trapping; crop monitoring; rice fields

1. Introduction

The increase in the concentration of carbon dioxide (CO$_2$) in the atmosphere is one of the main factors responsible for global warming. Currently, CO$_2$ levels are at 419 ppm; this represents 150% of the values in the 18th century [1]. This increase is mainly due to anthropogenic activities such as intensive agriculture and changes in land use, among others [2]. Rice (*Oryza sativa*) cultivation extends from tropical to temperate regions [3]. It is the second most important staple food in the world, with an annual production of 740 Mt [4]. It covers 114 countries and an area of 153 Mha in total, or 11% of the world's arable land [5]. In 2021, Peru produced 3.5 Mt of rice in an area of 417,000 ha [6]. Currently, 90% of rice production is obtained through flood irrigation [7], making it a significant source of methane (CH$_4$). Furthermore, nitrous oxide (N$_2$O) is mainly generated by nitrification and denitrification processes, which are closely related to soil moisture [8]. Both gases represent approximately 30% and 11%, respectively, of global agricultural emissions [9].

Net Ecosystem Exchange (NEE) is one of the main processes that influence CO_2 concentration in the atmosphere. Agricultural ecosystems, particularly rice paddies, play a crucial role in carbon absorption. Therefore, it is important to understand their function in carbon (C) flux [10]. For example, Chatterjee et al. [11] monitored lowland paddy fields for one year (dry and wet seasons) using eddy covariance (EC) to evaluate variations in NEE and find a suitable model for the better partitioning of NEE with respect to its components, such as gross primary production (GPP) and ecosystem respiration (Reco). Kumar et al. [12] calculated NEE in rice and wheat systems in the northwest Indo-Gangetic plains. This was the first estimation in a rice–wheat spring sequence using EC. Neogi et al. [13] investigated the characterization of CO_2 fluxes in tropical lowland rice paddy ecosystems using EC to better understand the environmental impact in terms of C budget in submerged soil.

The land–atmosphere exchange of matter and energy is recorded using EC [14], widely used given its solid theoretical basis. However, it is expensive, difficult to manipulate [15], and susceptible to information gaps [16]. On the other hand, static chambers are used to complement the deficiencies of EC. Nevertheless, they require long monitoring periods [17]. Additionally, the cost of chromatographic analysis for collected gases is high. In this regard, infrared sensors represent an opportunity to solve these challenges. They utilize the non-dispersive infrared (NDIR) principle to measure the concentration of CO_2 instantly [18]. In addition, they are easy to acquire, manipulate, and program. An automatic estimation and sampling method based on sensors that can replace the conventional methods mentioned and simultaneously increase the efficiency in estimating greenhouse gas (GHG) fluxes is necessary [19].

In this research, a CO_2 analyzer was designed together with a static chamber to monitor diurnal and nocturnal NEE in rice fields. The objective was to establish a novel, efficient, and dependable method of making resource management decisions for sustainable agricultural practices in Peru.

2. Materials and Methods

2.1. Site Description

This research was carried out in the "Experimental Irrigation Area" (AER) on the campus of the National Agrarian University La Molina (UNALM), La Molina District, Lima Province, Lima Region (12°04′41″ S, 76°56′45″ W, altitude: 246 m) (Figure 1). During the study, the maximum, minimum, and average temperatures were 32.3, 15.6, and 23.24 °C, respectively. The maximum precipitation was 2.6 mm with an average relative humidity of 77%. The meteorological data were recorded using the automatic station VANTAGE Pro2 Davis, Hayward, CA, USA, located at the AER (Figure 2). In addition, the physicochemical characteristics of the soil are detailed in Table 1.

Table 1. Physicochemical characteristics of the soil in the study area.

Variables	Value
Texture	Loam
σ $(dS\,m^{-1})$	0.37
pH	7.96
C.I.C $\left(mEq\,100\,g^{-1}\right)$	10.40
S.O.M. (%)	3.65
Apparent density $\left(g\,cm^{-3}\right)$	1.318
Real density $\left(g\,cm^{-3}\right)$	2.74
Porosity (%)	51.89
Field capacity $\left(cm^3\,cm^{-3}\right)$	19.91
Wilting point $\left(cm^3\,cm^{-3}\right)$	13.91
$CaCO_3$ (%)	4.02
P (ppm)	72.4
K^+ (ppm)	208
Total N (%)	0.21

σ = electric conductivity, pH = hydrogen potential, C.I.C = cation exchange capacity, S.O.M. = soil organic matter, $CaCO_3$ = calcium carbonate, P = phosphorus, K^+ = potassium ion, Total N = total nitrogen.
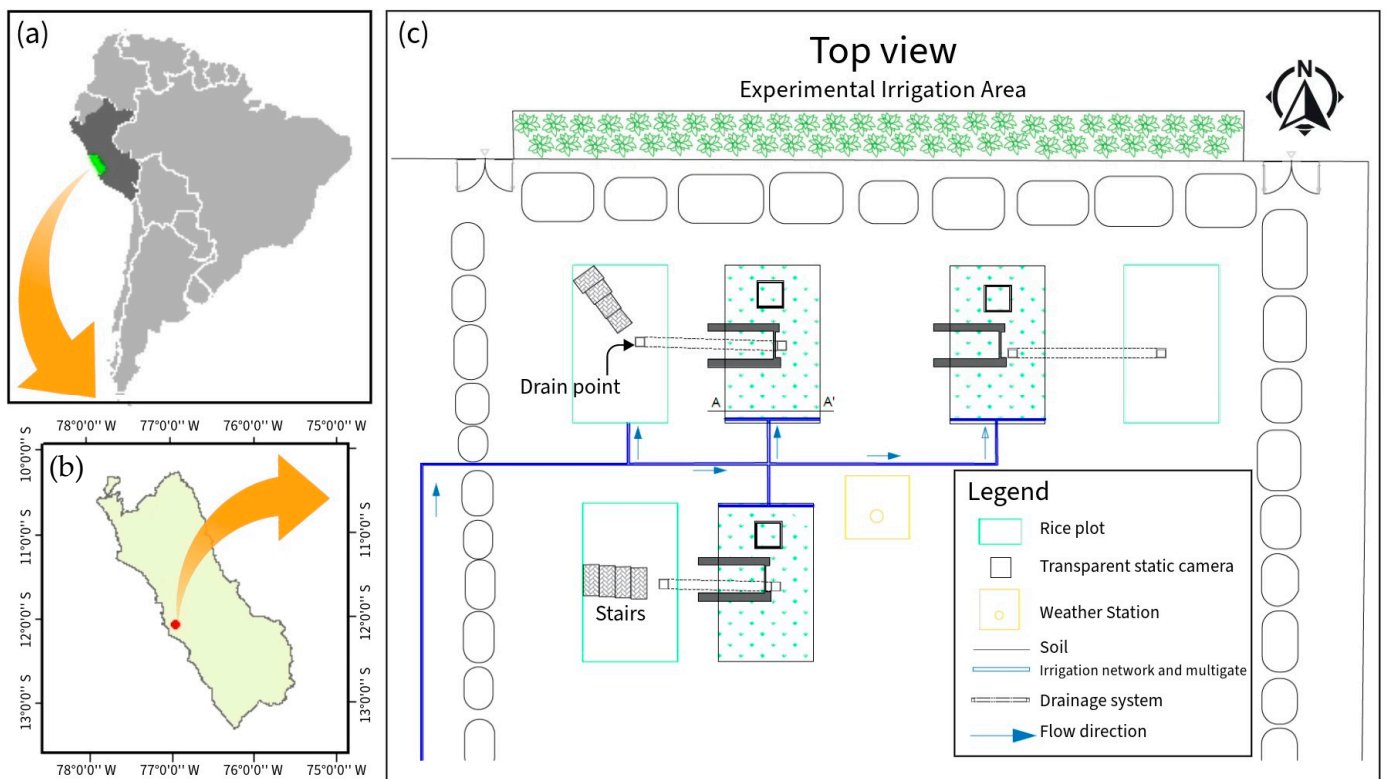
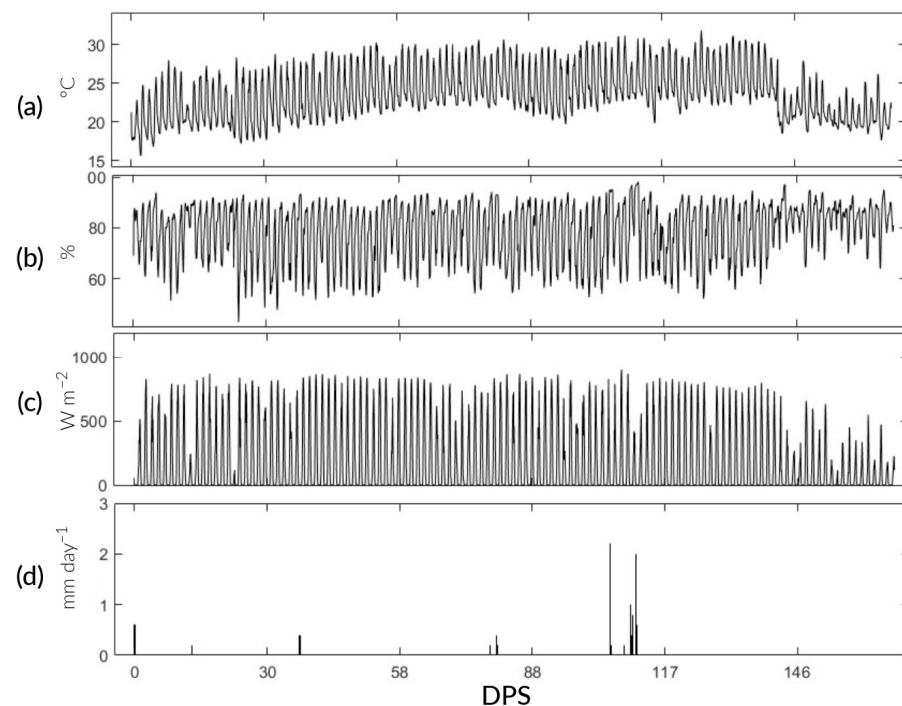**Figure 1.** (**a**,**b**) Location of the study area in Lima, Peru. (**c**) AER map.

Figure 2. Predominant climatic conditions during the study. (**a–d**) Air temperature (T_a), relative humidity (RH), net radiation (R_n), and precipitation (pp).

2.2. Design of Portable Analyzer for CO_2 Monitoring

A portable analyzer was designed for CO_2 monitoring (Figure 3a). Its components are as follows: (a) MHZ19B CO_2 sensor from Winsen Electronics; its detection range is 0 to 5000 ± 50 ppm. It operates at optimal T_a and RH conditions of 0 to 50 °C and 0 to

90%, respectively. (b) DHT22 T_a and RH sensor from Aosong Electronics. Its measurement range for T_a is -40 to 80 ± 0.5 °C, and for RH, it is 0 to 100 ± 2%. (c) Real-time clock (RTC) module "DS3231" from MMJ Smart Electronics. (d) microSD memory module from Deeoee Electronics. (e) 16×2 LED display from Yuxian Electronics. The Arduino DUE board (g) and "Arduino IDE", both from Arduino CC, were selected as the microcontroller unit and coding system, respectively. The components were soldered onto a multipurpose board (f) to ensure connection with the ARDUINO board. Then, the system was placed in a plastic box measuring $150 \times 110 \times 80$ mm^3. The device was powered by a PHILLIPS 4000 (mAh) portable battery with 5 V of output. The operational analyzer is shown in Figure 3b.
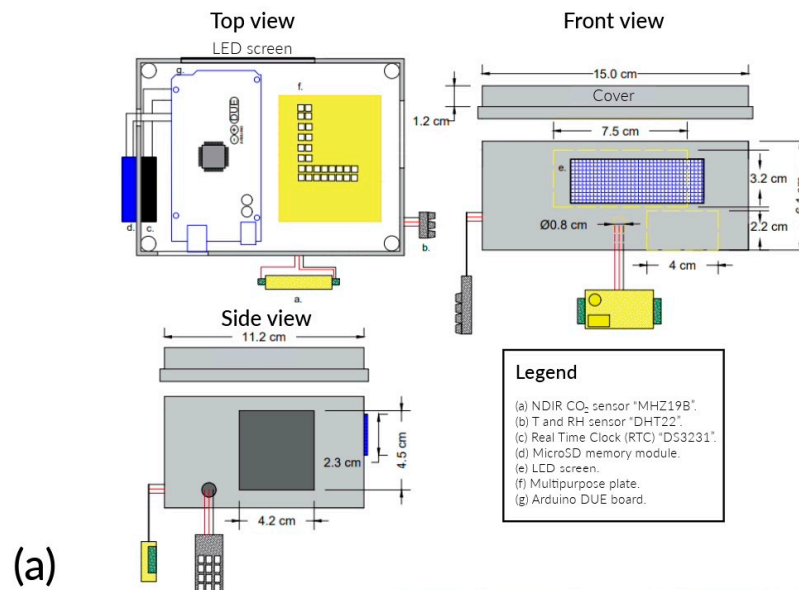

Figure 3. (**a**) Scheme of the portable analyzer for CO_2 monitoring; (**b**) analyzer finished.

2.3. Static Transparent Chamber Design

The monitoring system consisted of a static chamber and a portable CO_2 analyzer (Figure 4a). The chamber is made of transparent 2 mm thick transparent acrylic, whose dimensions are $1 \times 0.5 \times 0.5$ m^3. The gas-mixing system consisted of a portable battery (e) and 2 fans (f), both connected through a Universal Serial Bus (USB) port (g). In addition, the metal base, with dimensions of $0.5 \times 0.5 \times 0.15$ m^3, has a 2 mm thick slot. This was installed 6 cm below the soil surface before transplanting permanently. In addition, the analyzer is attached to one of the side faces using a support (h). The finished device is shown in Figure 4b.
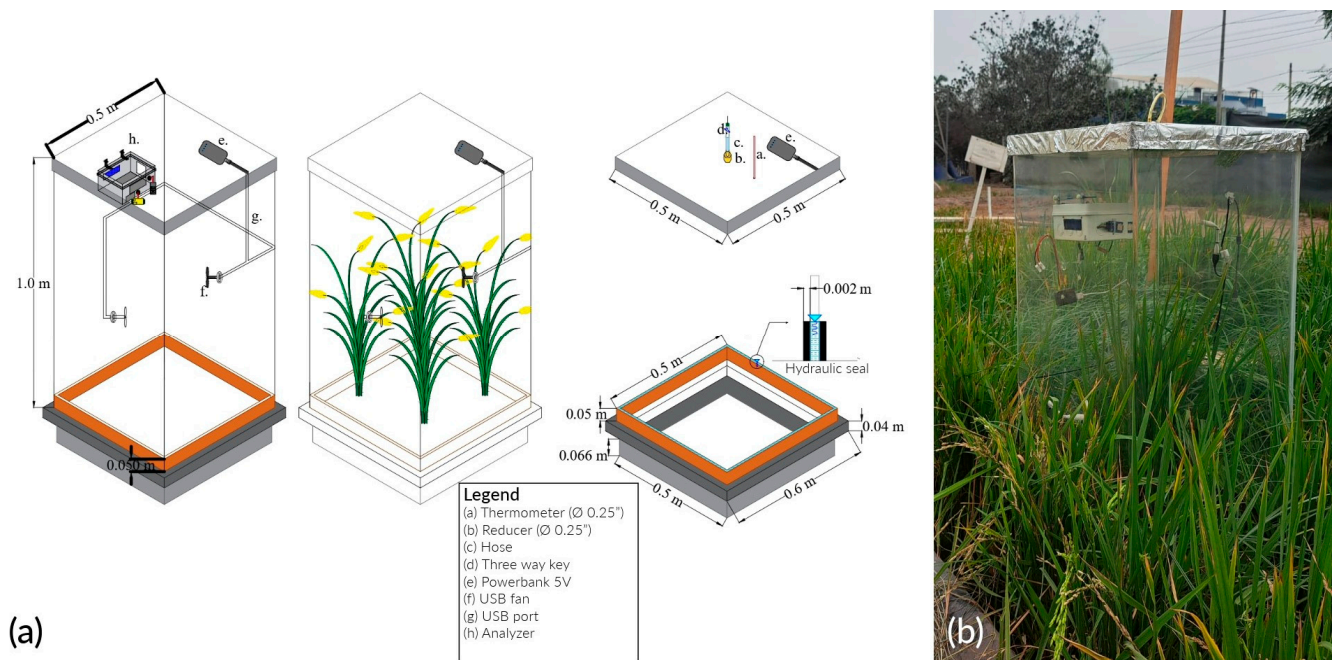
Figure 4. Transparent static chamber: (**a**) scheme; (**b**) disposition.

2.4. Field Management

Three ponds of $3 \times 4 \times 0.6$ m^3 were installed and lined with geomembrane (Figure 5a,b). The seedbed was prepared on 11 November 2022 and transplanted 35 days post-sowing (DPS). The distribution was five rice seedlings per hill, spaced 20 cm $\times$ 20 cm each. The vegetative, reproductive, and maturation phases lasted 95, 35, and 42 DPS, respectively. In total, the crop lasted 172 DPS (Figure 5c). The water regime maintained soil moisture between saturation and a 5 cm depth. Irrigation water came from the Rimac River and was stored in a 25 m^3 tank. Its physicochemical characteristics are described in Table 2. The NPK fertilization dose was 230-60-90. In total, 100% of P and K and 50% of N were applied during transplanting. The remaining N was distributed during tillering, floral primordium, and flowering (Figure 5d). The nitrogen sources were urea, diammonium phosphate (DAP), and "Basacote plus 3M".
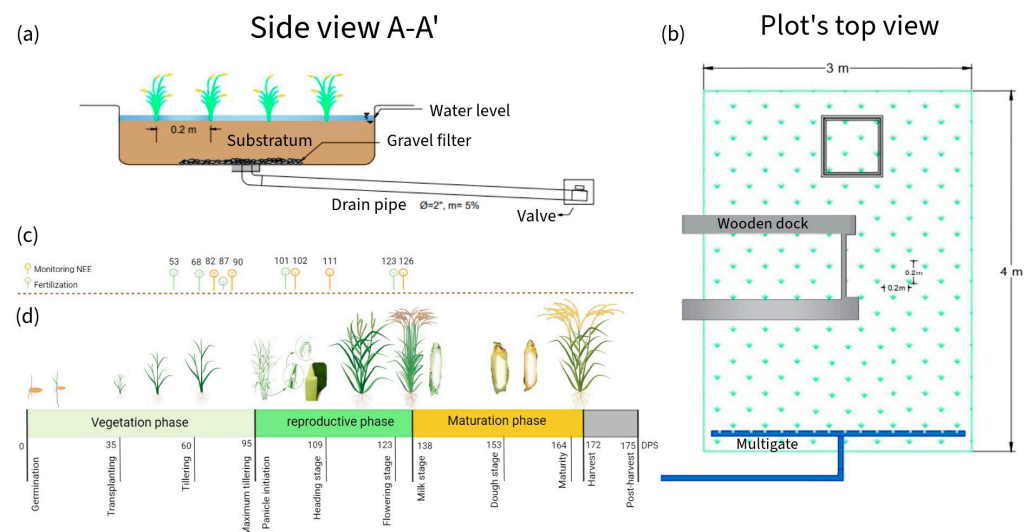

Figure 5. (**a**,**b**) Rice plot's side and top view, respectively (**c**) Calendar of monitoring and fertilization days (in DPS); (**d**) stages of rice paddy growth.

Table 2. Physicochemical characteristics of water.

Variables	Value
pH	8.2
σ (dS m^{-1})	0.67
Ca^{2+} (meq L^{-1})	4.38
Mg^{2+} (meq L^{-1})	0.68
Na^{+} (meq L^{-1})	1.76
K^{+} (meq L^{-1})	0.17
Cl^{-1} (meq L^{-1})	1.57
CO$_3{}^{2-}$ (meq L^{-1})	0.10
HCO$_3{}^{2-}$ (meq L^{-1})	3.01
SO$_4{}^{2-}$ (meq L^{-1})	2.13

pH = hydrogen potential, σ = electric conductivity, Ca^{2+} = calcium ion, Mg^{2+} = magnesium ion, Na^{+} = sodium ion, K^{+} = potassium ion, Cl^{-1} = chloride ion, CO$_3{}^{2-}$ = carbonate ion, HCO$_3{}^{2-}$ = bicarbonate, ion SO$_4{}^{2-}$ = sulfate ion.

2.5. Sensor Calibration

The MHZ19B sensor was calibrated with an automatic reference of 400 ppm by the manufacturer [20]. The DHT22 sensor was calibrated by relating its readings to the hourly data obtained by the automatic weather station for 24 h (Figure 6).
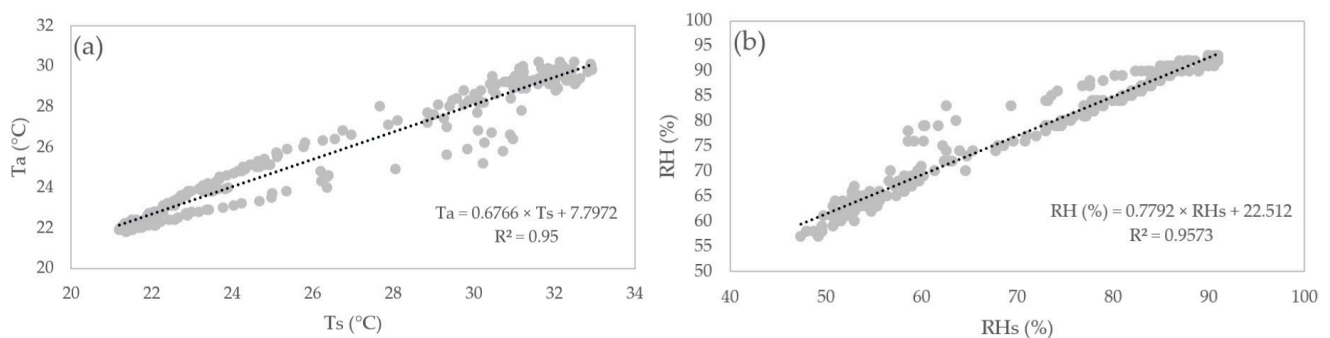
Figure 6. Correlation graph between the DHT22 sensor and the automatic station. (**a**) T$_a$; (**b**) RH.

T$_a$ is air temperature, T$_s$ is the air temperature reading by the sensor, RH is relative humidity, and RHs is the relative humidity reading by the sensor.

2.6. Monitoring and Data Collection

Diurnal CO$_2$ monitoring in rice plots begins at tillering, the stage of maximum leaf growth. There were 5 days that lasted 24 h each and were carried out simultaneously in the three plots. The preparatory phase began with the attachment of the static camera to the metal base. Then, a water seal was made on the coupling to prevent gas leakage. The analyzer was then placed and turned on in the chamber so that the CO$_2$, Ta, and RH readings stabilized for 30 min. Monitoring per se began with closing the chamber and turning on the fans during the first 30 min of each hour. The opposite action was carried out during the remaining 30 min.

2.7. Data Processing

Emission fluxes were calculated based on CO_2 concentration changes (ppm min^{-1}). Firstly, linear regression analysis was performed on 30 data [21,22]. Secondly, the CO_2 emission flux (μmol m^{-2} d^{-1}) was calculated with Equations (1)–(3).

$$\text{Flux}(CO_2) = K \times S \tag{1}$$

$$K = \frac{86400 \times P}{10^6 \times R \times T_c} \times \frac{V}{A} \tag{2}$$

$$S = \frac{\Delta C}{\Delta t} \tag{3}$$

where K is the accumulation factor of the chamber (mol min ppm^{-1} m^{-2} d^{-1}); S is the rate of change in CO_2 concentration (ppm min^{-1}); P is barometric pressure (mbar); R is the ideal gas constant, 0.0831451 (bar L K^{-1} mol^{-1}); T_c is the temperature inside the chamber (*K*); V is the net volume of the chamber (m^3); and A is the net area of the chamber entrance (m^2).

Thirdly, the Michaelis–Menten rectangular hyperbola model was used to calculate NEE [23]. The equation used was (4).

$$\text{NEE} = \frac{(\text{PPFD} \times -P_{\text{max}})}{K_m + \text{PPFD}} - R_{\text{eco}} \tag{4}$$

where NEE is the net CO_2 flux of the rice ecosystem $\left(\text{μmolCO2 m}^{-2}\text{ s}^{-1}\right)$, PPFD is the photosynthetic photon flux density $\left(\text{μmolphotons m}^{-2}\text{ s}^{-1}\right)$, P_{max} is the maximum photosynthetic rate, K_m is an adjustment constant, and Reco is the respiration rate of the rice ecosystems $\left(\text{μmolCO2 m}^{-2}\text{ s}^{-1}\right)$. For this, PPFD, P_{max}, and K_m data from Yang et al. [21] were used. The daily NEE for each phenological stage is the average of the fluxes from three analyzers. To verify the normality of the data, the Anderson–Darling test was used, which turned out to be non-parametric. Spearman correlation (*R*) was performed between the environmental variables, NEE, and Reco. Additionally, the Mann–Whitney U test was applied to assess significant differences between the results, at a significance level of 5%.

3. Results

3.1. Diurnal Variations in NEE

Figure 7 shows the diurnal behavior of NEE in the rice plots. The positive and negative signs indicate the net emission and absorption of CO_2, respectively. The maximum CO_2 emission at 89 and 102 DPS was at 4:00 and 6:00 a.m., whose values are 0.361 and 0.318 μmolCO2 m^2 s^{-1}. At 82, 111, and 126 DPS, it was at 18:00 with values of 0.68, 1, and 0.22 μmolCO2 m^2 s^{-1}. On the other hand, the maximum CO_2 assimilation occurred at 10:00 a.m., with values of −9.51, −9.25, −13.63, −12.9, and −12.5 μmolCO2 m^2 s^{-1} for 82, 89, 102, 111, and 126 DPS, respectively.

The total NEE was higher during the tillering stage on average (82 and 89 DPS), with −25.07 μmolCO2 m^2 s^{-1} on average. In floral primordium (102 DPS), it reached the minimum at −36.14 μmolCO2 m^2 s^{-1}. Then, it progressively increased during the spindle stage (111 DPS) at −34.98 μmolCO2 m^2 s^{-1} and the flowering stage (126 DPS) at −33.83 μmolCO2 m^2 s^{-1}. Likewise, the seasonal variations in NEE in the vegetative and reproductive phases were −25.07 and −34.98 μmolCO2 m^2 s^{-1}, respectively (Table 3).
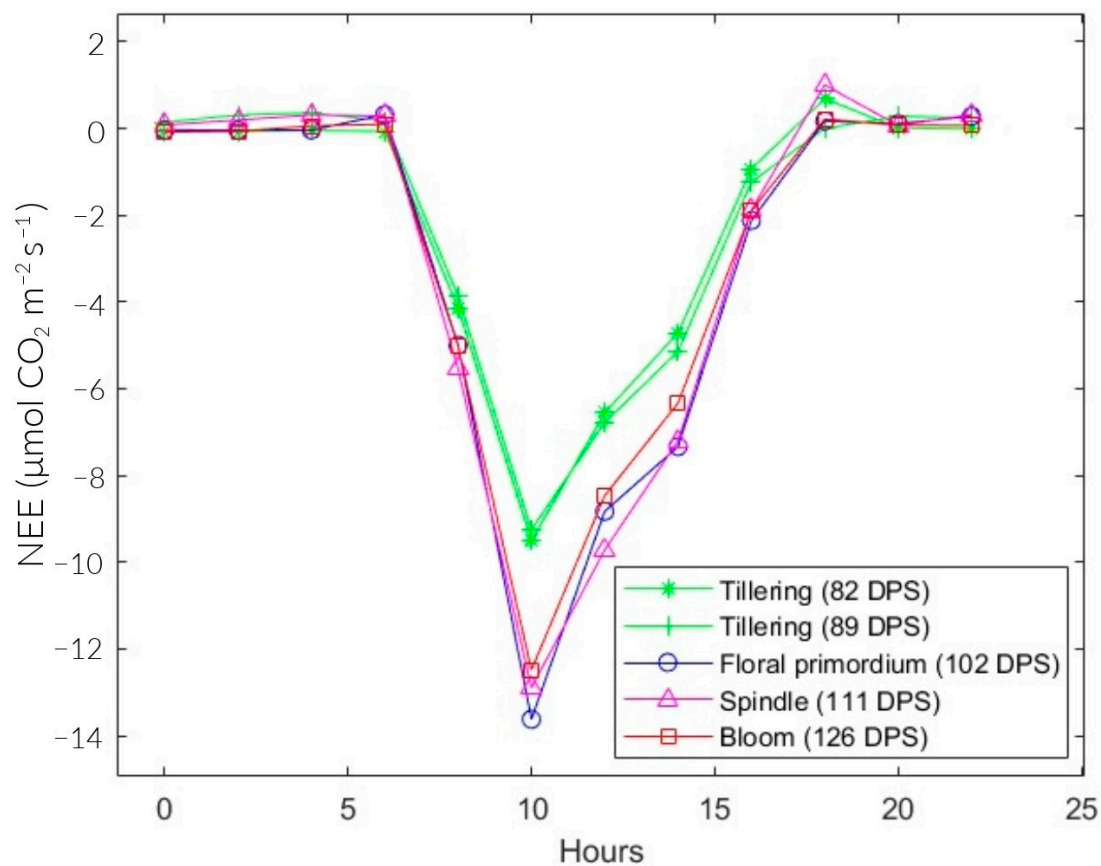
Figure 7. Diurnal NEE for different growth stages of rice fields.

Table 3. Diurnal NEE ($\mu molCO2\ m^2\ s^{-1}$) for different growth stages in rice fields.

Hour	PPFD Yang et al. [20]	DPS				
		82	89	102	111	126
0	10	-0.061 ± 0.09	0.143 ± 0.25	-0.034 ± 0.17	0.081 ± 0.19	-0.084 ± 0.15
2	10	-0.069 ± 0.05	0.309 ± 0.29	-0.041 ± 0.05	0.194 ± 0.25	-0.065 ± 0.19
4	10	-0.041 ± 0.12	0.361 ± 0.39	-0.036 ± 0.04	0.313 ± 0.47	0.059 ± 0.4
6	10	-0.064 ± 0.03	0.171 ± 0.21	0.318 ± 0.3	0.290 ± 0.47	0.097 ± 0.5
8	200	-4.148 ± 0.17	-3.860 ± 0.54	-4.997 ± 0.59	-5.550 ± 0.36	-5.021 ± 0.28
10	600	-9.511 ± 0.08	-9.245 ± 0.54	-13.626 ± 0.54	-12.901 ± 1.52	-12.489 ± 1.12
12	400	-6.555 ± 0.53	-6.777 ± 0.91	-8.829 ± 1.29	-9.720 ± 0.32	-8.468 ± 0.35
14	300	-4.710 ± 0.9	-5.141 ± 0.63	-7.336 ± 0.48	-7.202 ± 0.36	-6.330 ± 0.28
16	100	-0.928 ± 0.24	-1.233 ± 0.77	-2.123 ± 0.73	-1.881 ± 0.69	-1.899 ± 0.8
18	10	0.686 ± 0.89	-	0.171 ± 0.21	1.003 ± 0.6	0.218 ± 0.42
20	10	0.015 ± 0.18	0.280 ± 0.28	0.110 ± 0.09	0.069 ± 0.21	0.074 ± 0.28
22	10	-0.014 ± 0.04	0.247 ± 0.21	0.282 ± 0.24	0.321 ± 0.52	0.069 ± 0.3

3.2. NEE Response to Environmental Factors

The results of the Anderson–Darling test verified the non-normality of the data, except for Ts. Then, the correlations between the environmental factors, Reco, and NEE were analyzed. Coefficients close to 1 and -1 indicate strong positive and negative correlations, respectively (Figure 8). NEE was positively and significantly correlated with RH_c (R = 0.66, $p < 0.05$) and T_s (R = 0.26, $p < 0.05$). Furthermore, it showed a highly significant negative correlation with Rn (R = -0.75, $p < 0.05$) and T_c (R = -0.69, $p < 0.05$). On the other hand, Reco was highly positively associated with T_c (R = 0.7, $p < 0.05$) and Rn (R = 0.73, $p < 0.05$). In addition, it showed a significant negative correlation with RHc (R = -0.55, $p < 0.05$) and Ts (R = -0.4, $p < 0.05$).

Figure 8. Spearman correlation heat map (R) between NEE, Reco, and environmental variables. Light and dark colors indicate positive and negative correlations, respectively. "*" indicates a significant correlation at the 0.05 level ($p < 0.05$).

4. Discussion

4.1. Diurnal Variation in NEE

The NEE values during the study are represented in Figure 7. They are positive at night and negative during the day. This behavior is consistent with the results obtained by Bhattacharyya et al. [24], McMillan et al. [25], and Zhang et al. [26]. During daylight hours, the ecosystem functioned as a carbon dioxide (CO_2) sink, with higher levels of absorption through photosynthesis compared with emissions through respiratory processes. However, during the nighttime, the ecosystem acted as a source of CO_2, primarily because of Reco [27,28]. In the absence of sunlight, NEE is, on average, 58 times lower than the results of Yang et al. [21] and Bhattacharyya et al. [29]. This decrease can be attributed to the higher levels of RHc during the same period (Figure 9d). As a result, the sensor did not perform at its optimal level. In contrast to portable analyzer technology, the EC methodology used in the aforementioned studies employed open-path NDIR gas analyzers such as the LI-7200, LI-7500, and EC-150. These are specifically designed to measure fluxes in CO_2, water vapor, and energy below the canopy. Therefore, their prices are excessively higher compare with a portable analyzer. In this study, the "MHZ19B" NDIR sensor was used, which differs in application, precision, and price. However, if optimal operating conditions are guaranteed, the sensor has a high potential for accuracy and practicality.
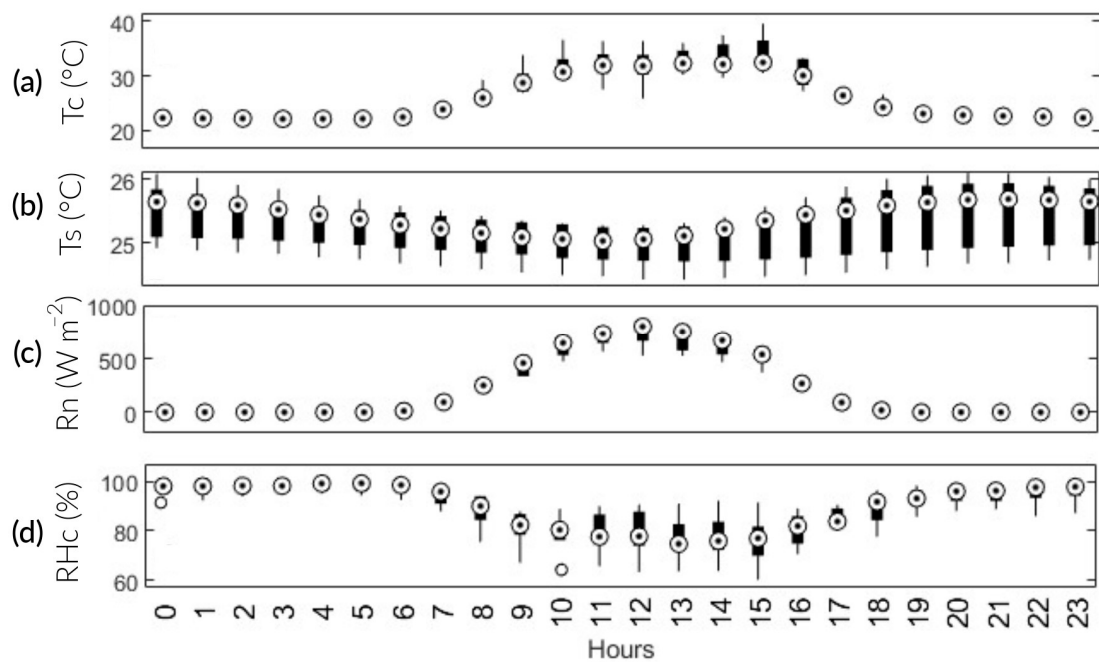
Figure 9. Boxplot graphic: average diurnal variation in the main environmental factors. (**a**) Tc; (**b**) Ts; (**c**) Rn; and (**d**) RHc.

On the other hand, total NEE during the vegetative phase (-25.2 μmolCO2 m^2 s^{-1}) was 1.4 times lower than the minimum during the reproductive phase (-35 μmolCO2 m^2 s^{-1}). Similarly, the maximum diurnal NEE during the reproductive stage (-13 μmolCO2 m^2 s^{-1}) was 1.4 times higher than during the vegetative stage (-9.4 μmolCO2 m^2 s^{-1}). This is consistent with Yang et al. [21], who determined that the maximum absorption during the vegetative and maturation phase was approximately 1.5 times lower than in the reproductive phase. In the vegetative phase, CO_2 assimilation is limited because the plant is in the growth stage (Figure 10a,b). In the reproductive stage, complete development is observed, leading to maximum absorption. In the maturation stage, senescent leaves fall and add organic matter to the soil. Additionally, the plots are drained in preparation for the harvest phase. These two processes gradually increase CO_2 emissions until the crop is harvested (Figure 10c,d). This behavior is similar to the results of Chen et al. [30].

Figure 10. Rice field growth in different stages of the cycle. (**a**–**d**) Tillering (82 and 89 DPS), spindle stage (111 DPS), and flowering (126 DPS).

4.2. NEE, Reco, and Their Interactions with Environmental Variables

The results for Reco showed a strong positive correlation with Tc and Rn. It is worth noting that these variables are strongly and positively related (R^2 = 0.84). According to previous studies, Tc is an important factor in CO_2 emissions from agricultural ecosystems [30,31]; the same applies to Rn. As Rn and Tc intensify throughout the day, root and microbial activity emits CO_2 into the atmosphere. The maximum Reco occurs at 12:00 p.m. Nevertheless, photosynthetic activity is higher than Reco. In comparison with Bao et al. [27], it was observed that Reco had a weak negative correlation with Ts, possibly influenced by soil texture, ecosystem type, and water regime. In contrast, the seasonal variation in NEE was negatively related to Tc and Rn. Rn plays a crucial role as the primary energy source for plant metabolism. Consequently, when there is an increase in available energy, plants will absorb more CO_2 (Figure 9c). These findings line up with the research conducted by Liu et al. [31].

Regarding Tc, the results are consistent with those of Bhattacharyya et al. [29] and Morales [32]. They found an inverse relationship between temperature and CO_2 assimilation after surpassing 34 °C. This is because the rubisco enzyme, which is essential in CO_2 fixation, is susceptible to thermal stress. Thus, the temperature inside the chamber exceeded this threshold at 82 DPS between 10:00 a.m. and 3:00 p.m. This may be a factor in why NEE is at its maximum throughout the season. Additionally, between 2:00 p.m. and 6:00 p.m., there is a 3.9-fold increase in CO_2 emissions (Figure 9a). There is a weak positive correlation between NEE and Ts. Ts, in turn, has a weak negative correlation with Tc. This partially agrees with Liu et al. [31], as they did find a significantly high effect between Tc and Ts.

4.3. Comparison with Previous Studies

Information about the environmental and field management conditions from other authors is summarized in Table 4, as they influence CO_2 absorption (Chen et al. [30] and Li et al. [33]).

Table 4. Main environmental characteristics of the studies involved.

Site	Köppen–Geiger Climate Classification	Field Management	Soil Texture	Reference
Cuttack, India	Tropical savanna (Aw)	Flood irrigation. Water depth: 8 cm.	Sandy clay loam	Chatterjee et al. [11]
Delhi, India	Warm semiarid (Bsh)	Conventional puddling.	Loam	Kumar et al. [12]
Cuttack, India	Tropical savanna (Aw)	Flood irrigation. Water depth: 7–10 cm.	Sandy clay loam	Neogi et al. [13]
Lima, Peru	Hot desert (Bwh)	Conventional puddling. Water depth: 5 cm.	Loam	-

The results (Figure 11, Tables A1–A4) indicate a lower capacity for CO_2 absorption than Chatterjee et al. [11], Kumar et al. [12], and Neogi et al. [13]; possibly influenced by climatic conditions. The study was under the conditions of a hot desert (Bwh) climate because of the permanent presence of the South Pacific anticyclone in northern Chile. On the other hand, Chatterjee et al. [11] and Neogi et al. [13] carried out their studies at the ICAR—National Rice Research Institute (NRRI) in India; they recorded climatic conditions typical of the tropical savanna type (Aw). For their part, Kumar et al. [12] at the Indian Agricultural Research Institute (IARI) in Dehli, India, were under hot semiarid climate conditions (Bsh).
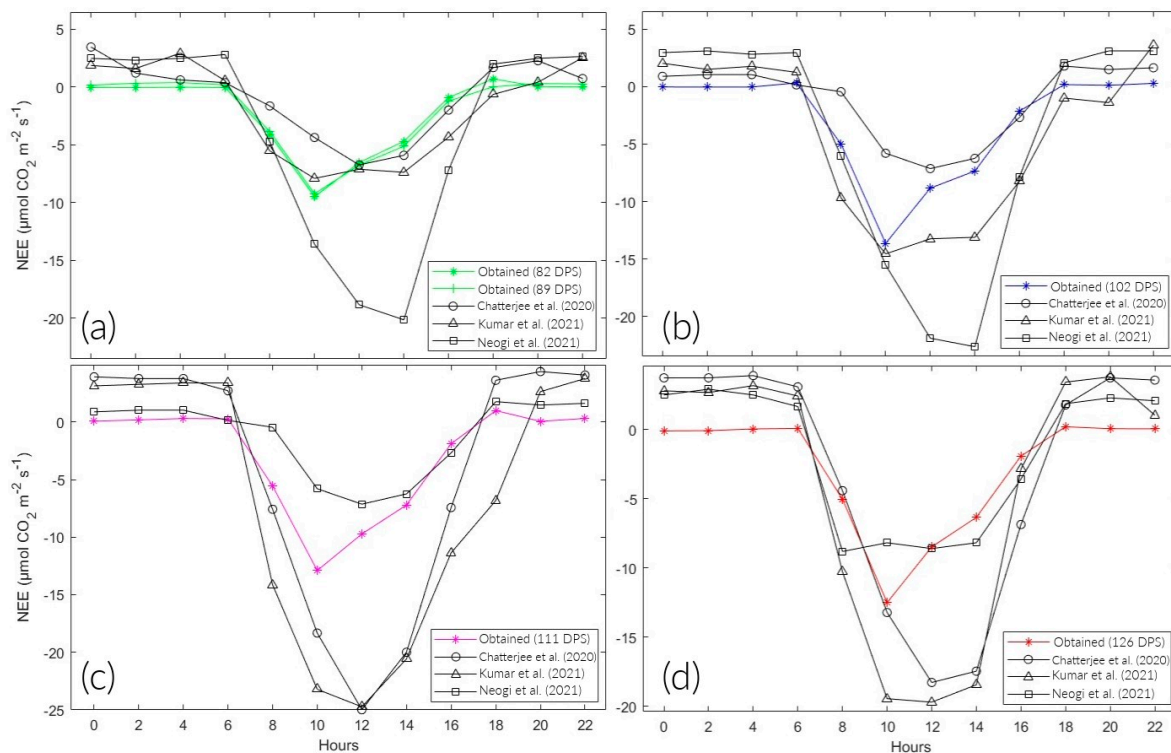
Figure 11. Comparison of the diurnal variation in NEE in different stages of the rice phenological cycle. (**a**–**d**) Tillering, floral primordium, spindle stage, and flowering, respectively, cited in Chatterjee et al. [11], Kumar et al. [12] & Neogi et al. [13].

Regarding pp during the rice season, a total of 13.4 mm was recorded, despite the influence of the cyclone "Yaku," which coincided with 111 and 126 DPS (Figure 2d). In comparison with Chatterjee et al. [11] and Neogi et al. [13], whose average annual pp was 1500 mm. 75 and 80% was happened between June and September. Kumar et al. [12], whose studies were carried out in Delhi, recorded 1198 mm during the kharif season for rice cultivation when most of the rains occur from July to September because of the southwest monsoon.

Regarding Tc, it ranged from 21.82 to 33.9 °C on average. On the other hand, Ts fluctuated between 24.95 and 25.51 °C on average. This study was carried out in the months of February to May during the summer season when the cold phase of the El Niño Southern Oscillation (ENSO) is also influential. Chatterjee et al. [11] recorded average annual maximum and minimum temperatures of 39.2 and 22.5 °C. Kumar et al. [12] recorded Ta and Ts values between 31.8 to 38.2 °C and 27.7 to 28.9 °C, respectively. Neogi et al. [13] recorded a progressive increase in temperature as the vegetative cycle of rice continued. From the vegetative stage to harvest, the average temperatures were 23.6 to 33.5 °C, respectively.

However, there were variations in the irrigation techniques used. This study had a maximum water depth of 5 cm during the entire study period. Chatterjee et al. [11] used a higher water regime in three units. Kumar et al. [12] irrigated their crops only when the moisture content fell below the saturation level. In turn, the irrigation regime of Neogi et al. [13] resulted in a sheet of 7–10 cm. According to Yang et al. [22], NEE is sensitive to field management strategies, with water management being one of the most important factors. In addition, soil CO_2 emissions decrease when flooded with water, as this reduces the diffusivity of the upper layer of soil [34]. These anoxic conditions decrease soil biological activity, as mentioned by Bao et al. [27] and Liu et al. [31]. The result obtained from the Mann–Whitney U test shows that the NEE values did not present a significant difference between the analyzed studies ($p > 0.05$). Therefore, the CO_2 analyzer generally

performed optimally throughout the 24 h of monitoring and throughout the entire study period. However, more research is needed to consider it a reference method (Table 5).

Table 5. Mann–Whitney U test for the values obtained compared with Chatterjee et al. [11], Kumar et al. [12], and Neogi et al. [13]. "*" indicates that there is no significant difference at the 0.05 level ($p \geq 0.05$).

References	Tillering		Floral Primordium	Spindle State	Bloom
	82 DPS	89 DDS	102 DPS	111 DPS	126 DPS
Chatterjee et al. [11]	96 **	98 **	99 **	88 **	90 **
Kumar et al. [12]	83 **	85 **	75 **	76 **	89 **
Neogi et al. [13]	87 **	88 **	89 **	96 **	94 **

4.4. Portable Analyzer Performance

The MHZ19B sensor has a response time of less than 60 s, so the analyzer was programmed with a response time of one minute to perform a better analysis. On the other hand, open-path analyzers such as LI—7500A and LI—7550 have selectable response times of 0.1, 0.05, and 0.0025 s [35]. In addition, a regression analysis was performed between NEE fluxes calculated from data collected with the portable analyzer and NEE fluxes calculated using EC by Chatterjee et al. [11], Kumar et al. [12], and Neogi et al. [13]. The determination coefficients have values of 0.661, 0.7873, and 0.5943, respectively (Figure 12). These values can be improved if an additional calibration method is taken into consideration and by improving the Tc and RHc conditions. Furthermore, the sensitivity of the sensors is also an important factor to consider since the MHZ19B has a sensitivity of ± 50 ppm compared with LI—7500A, with ± 0.11 ppm [35].
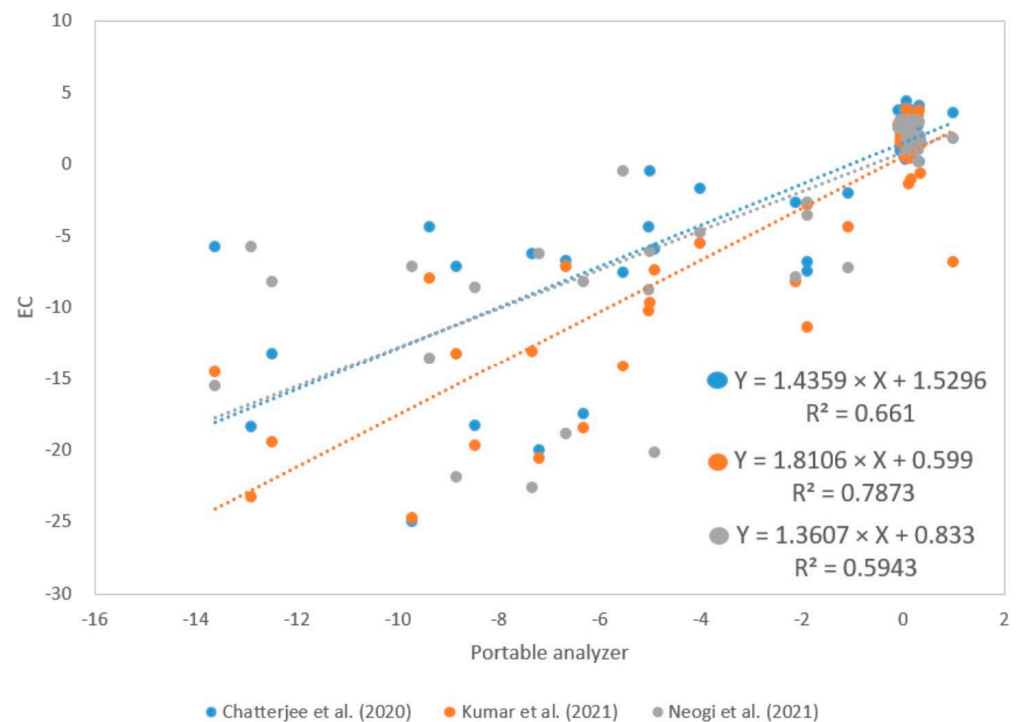

Figure 12. Determination coefficients between NEE values ($\mu molCO2\ m^2\ s^{-1}$) calculated with the portable analyzer and EC by Chatterjee et al. [11], Kumar et al. [12] & Neogi et al. [13]; respectively.

5. Conclusions

A static chamber with a portable CO_2 analyzer was designed and implemented. It is an economical, simple, and effective alternative to traditional NEE calculation methods. It

is a useful tool for making decisions about resource management in agricultural practice in Peru. Rice plots acted as a CO_2 sink from 6:00 a.m. to 6:00 p.m. and as a CO_2 source during the remaining period. The minimum NEE values at 82, 89, 102, 111, and 126 DPS were -9.51, -9.25, -13.63, -12.9, and -12.5 μmolCO2 m^2 s^{-1}; the maximum NEE values for the same dates were 0.68, 0.36, 0.32, 1, and 0.22 μmolCO2 m^2 s^{-1}, respectively.

The total seasonal NEE values were -25.2 and -34.98 μmolCO2 m^2 s^{-1} for the growth and reproductive stages, respectively. This represents a difference of 1.4 times between the mentioned stages. On the other hand, NEE was mainly influenced by Rn (R = -0.75), Tc (R = -0.69), and RHc (R = 0.66). NEE was negative throughout the rice growth period, demonstrating that the rice field acted as a net CO_2 sink. The results did not show a significant difference compared with previous studies, indicating the optimal performance of the analyzer. Furthermore, differences in CO_2 absorption can primarily be attributed to the type of crop, irrigation management, and climatic and soil conditions. These results are similar to previous studies obtained via chromatographic analysis and eddy covariance (EC), which suggests that the portable analyzer could be an alternative for CO_2 monitoring.

Institutional Review Board Statement: Not applicable.

Informed Consent Statement: Not applicable.

Data Availability Statement: The data presented in this study are available on request from the corresponding author.

Conflicts of Interest: The authors declare no conflicts of interest.

Appendix A

Table A1. Comparison of the diurnal variation in NEE (μmolCO2 m^2 s^{-1}) in tillering.

Hour	PPFD Yang et al. [21]	DPS		References		
		82	89	Chatterjee et al. [11]	Kumar et al. [12]	Neogi et al. [13]
0	10	-0.061 ± 0.09	0.143 ± 0.25	3.439	1.84	2.459
2	10	-0.069 ± 0.05	0.309 ± 0.29	1.186	1.58	2.295
4	10	-0.041 ± 0.12	0.361 ± 0.39	0.593	2.91	2.459
6	10	-0.064 ± 0.03	0.171 ± 0.21	0.356	0.53	2.787
8	200	-4.148 ± 0.17	-3.860 ± 0.54	-1.660	-5.55	-4.754
10	600	-9.511 ± 0.08	-9.245 ± 0.54	-4.387	-7.93	-13.607
12	400	-6.555 ± 0.53	-6.777 ± 0.91	-6.759	-7.14	-18.852
14	300	-4.710 ± 0.9	-5.141 ± 0.63	-5.929	-7.40	-20.164
16	100	-0.928 ± 0.24	-1.233 ± 0.77	-2.016	-4.36	-7.213
18	10	0.686 ± 0.89	-	1.660	-0.66	1.967
20	10	0.015 ± 0.18	0.280 ± 0.28	2.253	0.40	2.459
22	10	-0.014 ± 0.04	0.247 ± 0.21	0.711	2.51	2.623

Table A2. Comparison of the diurnal variation in NEE ($\mu molCO2\ m^2\ s^{-1}$) in floral primordium.

Hour	PPFD Yang et al. [21]	DPS 102	References Chatterjee et al. [11]	Kumar et al. [12]	Neogi et al. [13]
0	10	-0.034 ± 0.17	0.891	2.03	2.956
2	10	-0.041 ± 0.05	1.040	1.50	3.103
4	10	-0.036 ± 0.04	1.040	1.76	2.808
6	10	0.318 ± 0.3	0.149	1.24	2.956
8	200	-4.997 ± 0.59	-0.446	-9.68	-6.059
10	600	-13.626 ± 0.54	-5.792	-14.55	-15.517
12	400	-8.829 ± 1.29	-7.129	-13.23	-21.872
14	300	-7.336 ± 0.48	-6.238	-13.10	-22.611
16	100	-2.123 ± 0.73	-2.673	-8.23	-7.833
18	10	0.171 ± 0.21	1.782	-1.00	2.069
20	10	0.110 ± 0.09	1.485	-1.39	3.103
22	10	0.282 ± 0.24	1.634	3.60	3.103

Table A3. Comparison of the diurnal variation in NEE ($\mu molCO2\ m^2\ s^{-1}$) in spindle state.

Hour	PPFD Yang et al. [21]	DPS 111	References Chatterjee et al. [11]	Kumar et al. [12]	Neogi et al. [13]
0	10	0.081 ± 0.19	3.939	3.15	0.891
2	10	0.194 ± 0.25	3.788	3.28	1.040
4	10	0.313 ± 0.47	3.788	3.41	1.040
6	10	0.290 ± 0.47	2.727	3.41	0.149
8	200	-5.550 ± 0.36	-7.576	-14.14	-0.446
10	600	-12.901 ± 1.52	-18.333	-23.23	-5.792
12	400	-9.720 ± 0.32	-25.000	-24.75	-7.129
14	300	-7.202 ± 0.36	-20.000	-20.58	-6.238
16	100	-1.881 ± 0.69	-7.424	-11.36	-2.673
18	10	1.003 ± 0.6	3.636	-6.82	1.782
20	10	0.069 ± 0.21	4.394	2.65	1.485
22	10	0.321 ± 0.52	4.091	3.79	1.634

Table A4. Comparison of the diurnal variation in NEE ($\mu molCO2\ m^2\ s^{-1}$) in bloom.

Hour	PPFD Yang et al. [21]	DPS 126	References Chatterjee et al. [11]	Kumar et al. [12]	Neogi et al. [13]
0	10	-0.084 ± 0.15	3.750	2.82	2.513
2	10	-0.065 ± 0.19	3.750	2.69	2.932
4	10	0.059 ± 0.4	3.913	3.19	2.513
6	10	0.097 ± 0.5	3.098	2.44	1.675
8	200	-5.021 ± 0.28	-4.402	-10.26	-8.796
10	600	-12.489 ± 1.12	-13.207	-19.43	-8.168
12	400	-8.468 ± 0.35	-18.261	-19.69	-8.586
14	300	-6.330 ± 0.28	-17.446	-18.43	-8.168
16	100	-1.899 ± 0.8	-6.848	-2.84	-3.560
18	10	0.218 ± 0.42	1.793	3.44	1.885
20	10	0.074 ± 0.28	3.750	3.82	2.304
22	10	0.069 ± 0.3	3.587	1.06	2.094

References

1. Change, N.G.C. Carbon Dioxide Concentration | NASA Global Climate Change. Available online: https://climate.nasa.gov/vital-signs/carbon-dioxide (accessed on 29 December 2023).
2. Zhang, Y.; Liu, H.; Qi, J.; Feng, P.; Zhang, X.; Liu, D.L.; Marek, G.W.; Srinivasan, R.; Chen, Y. Assessing Impacts of Global Climate Change on Water and Food Security in the Black Soil Region of Northeast China Using an Improved SWAT-CO2 Model. *Sci. Total Environ.* **2023**, *857*, 159482. [CrossRef] [PubMed]

3. Oo, A.Z.; Yamamoto, A.; Ono, K.; Umamageswari, C.; Mano, M.; Vanitha, K.; Elayakumar, P.; Matsuura, S.; Bama, K.S.; Raju, M.; et al. Ecosystem Carbon Dioxide Exchange and Water Use Efficiency in a Triple-Cropping Rice Paddy in Southern India: A Two-Year Field Observation. *Sci. Total Environ.* **2023**, *854*, 158541. [CrossRef] [PubMed]

4. Kumar, A.; Nayak, A.K.; Das, B.S.; Panigrahi, N.; Dasgupta, P.; Mohanty, S.; Kumar, U.; Panneerselvam, P.; Pathak, H. Effects of Water Deficit Stress on Agronomic and Physiological Responses of Rice and Greenhouse Gas Emission from Rice Soil under Elevated Atmospheric CO_2. *Sci. Total Environ.* **2019**, *650*, 2032–2050. [CrossRef] [PubMed]

5. Gupta, K.; Kumar, R.; Baruah, K.K.; Hazarika, S.; Karmakar, S.; Bordoloi, N. Greenhouse Gas Emission from Rice Fields: A Review from Indian Context. *Environ. Sci. Pollut. Res.* **2021**, *28*, 30551–30572. [CrossRef]

6. FAOSTAT. Available online: https://www.fao.org/faostat/es/#data/QCL (accessed on 29 December 2023).

7. Gao, H.; Liu, Q.; Yan, C.; Wu, Q.; Gong, D.; He, W.; Liu, H.; Wang, J.; Mei, X. Mitigation of Greenhouse Gas Emissions and Improved Yield by Plastic Mulching in Rice Production. *Sci. Total Environ.* **2023**, *880*, 162984. [CrossRef]

8. Liao, B.; Cai, T.; Wu, X.; Luo, Y.; Liao, P.; Zhang, B.; Zhang, Y.; Wei, G.; Hu, R.; Luo, Y.; et al. A Combination of Organic Fertilizers Partially Substitution with Alternate Wet and Dry Irrigation Could Further Reduce Greenhouse Gases Emission in Rice Field. *J. Environ. Manag.* **2023**, *344*, 118372. [CrossRef]

9. Gangopadhyay, S.; Chowdhuri, I.; Das, N.; Pal, S.C.; Mandal, S. The Effects of No-Tillage and Conventional Tillage on Greenhouse Gas Emissions from Paddy Fields with Various Rice Varieties. *Soil Tillage Res.* **2023**, *232*, 105772. [CrossRef]

10. Yang, S.; Sun, X.; Ding, J.; Jiang, Z.; Liu, X.; Xu, J. Effect of Biochar Addition on CO_2 Exchange in Paddy Fields under Water-Saving Irrigation in Southeast China. *J. Environ. Manag.* **2020**, *271*, 111029. [CrossRef]

11. Chatterjee, S.; Swain, C.K.; Nayak, A.K.; Chatterjee, D.; Bhattacharyya, P.; Mahapatra, S.S.; Debnath, M.; Tripathi, R.; Guru, P.K.; Dhal, B. Partitioning of Eddy Covariance-Measured Net Ecosystem Exchange of CO_2 in Tropical Lowland Paddy. *Paddy Water Environ.* **2020**, *18*, 623–636. [CrossRef]

12. Kumar, A.; Bhatia, A.; Sehgal, V.K.; Tomer, R.; Jain, N.; Pathak, H. Net Ecosystem Exchange of Carbon Dioxide in Rice-Spring Wheat System of Northwestern Indo-Gangetic Plains. *Land* **2021**, *10*, 701. [CrossRef]

13. Neogi, S.; Bhattacharyya, P.; Nayak, A.K. Characterization of Carbon Dioxide Fluxes in Tropical Lowland Flooded Rice Ecology. *Paddy Water Environ.* **2021**, *19*, 539–552. [CrossRef]

14. Klosterhalfen, A.; Chi, J.; Kljun, N.; Lindroth, A.; Laudon, H.; Nilsson, M.B.; Peichl, M. Two-Level Eddy Covariance Measurements Reduce Bias in Land-Atmosphere Exchange Estimates over a Heterogeneous Boreal Forest Landscape. *Agric. For. Meteorol.* **2023**, *339*, 109523. [CrossRef]

15. Zhao, Y.; Wu, J.; Guo, C.; Wu, H.; Wang, J.; Zhang, Q.; Xiao, Y.; Qiu, R. Comparing the Eddy Covariance and Gradient Methods for Measuring Water and Heat Fluxes in Paddy Fields. *Agric. Water Manag.* **2023**, *284*, 108340. [CrossRef]

16. Gao, D.; Yao, J.; Yu, S.; Ma, Y.; Li, L.; Gao, Z. Eddy Covariance CO_2 Flux Gap Filling for Long Data Gaps: A Novel Framework Based on Machine Learning and Time Series Decomposition. *Remote Sens.* **2023**, *15*, 2695. [CrossRef]

17. Li, J.; Xue, Z.; Li, Y.; Bo, G.; Shen, F.; Gao, X.; Zhang, J.; Tan, T. Real-Time Measurement of Atmospheric CO_2, CH_4 and N_2O above Rice Fields Based on Laser Heterodyne Radiometers (LHR). *Agronomy* **2023**, *13*, 373. [CrossRef]

18. Low-Cost IoT-Enabled Embedded System for Measurement of Environmental Pollutants—ProQuest. Available online: https://www.proquest.com/openview/98d3b4da3c59b80ae4541e3b6eb9ea60/1?pq-origsite=gscholar&cbl=2030013 (accessed on 29 December 2023).

19. Rajasekar, P.; Selvi, J.A.V. Sensing and Analysis of Greenhouse Gas Emissions from Rice Fields to the Near Field Atmosphere. *Sensors* **2022**, *22*, 4141. [CrossRef] [PubMed]

20. Coulby, G.; Clear, A.K.; Jones, O.; Godfrey, A. Low-Cost, Multimodal Environmental Monitoring Based on the Internet of Things. *Build. Environ.* **2021**, *203*, 108014. [CrossRef]

21. Yang, S.; Xu, J.; Liu, X.; Zhang, J.; Wang, Y. Variations of Carbon Dioxide Exchange in Paddy Field Ecosystem under Water-Saving Irrigation in Southeast China. *Agric. Water Manag.* **2016**, *166*, 42–52. [CrossRef]

22. Yang, S.; Liu, X.; Liu, X.; Xu, J. Effect of Water Management on Soil Respiration and NEE of Paddy Fields in Southeast China. *Paddy Water Environ.* **2017**, *15*, 787–796. [CrossRef]

23. Pilegaard, K.; Hummelshøj, P.; Jensen, N.O.; Chen, Z. Two Years of Continuous CO_2 Eddy-Flux Measurements over a Danish Beech Forest. *Agric. For. Meteorol.* **2001**, *107*, 29–41. [CrossRef]

24. Bhattacharyya, P.; Neogi, S.; Roy, K.S.; Dash, P.K.; Nayak, A.K.; Mohapatra, T. Tropical Low Land Rice Ecosystem Is a Net Carbon Sink. *Agric. Ecosyst. Environ.* **2014**, *189*, 127–135. [CrossRef]

25. McMillan, A.M.S.; Goulden, M.L.; Tyler, S.C. Stoichiometry of CH_4 and CO_2 Flux in a California Rice Paddy. *J. Geophys. Res. Biogeosci.* **2007**, *112*, G01008. [CrossRef]

26. Carbon Dioxide Fluxes over Grassland Ecosystems in the Middle Tianshan Region of China with Eddy Covariance Method. Available online: https://www.researchsquare.com (accessed on 29 December 2023).

27. Bao, Y.; Liu, T.; Duan, L.; Tong, X.; Zhang, Y.; Wang, G.; Singh, V.P. Variations and Controlling Factors of Carbon Dioxide and Methane Fluxes in a Meadow-Rice Ecosystem in a Semi-Arid Region. *CATENA* **2022**, *215*, 106317. [CrossRef]

28. Chatterjee, D.; Swain, C.K.; Chatterjee, S.; Bhattacharyya, P.; Tripathi, R.; Lal, B.; Gautam, P.; Shahid, M.; Dash, P.K.; Dhal, B.; et al. Is the Energy Balance in a Tropical Lowland Rice Paddy Perfectly Closed? *Atmósfera* **2021**, *34*, 59–78. [CrossRef]

29. Net Ecosystem CO_2 Exchange and Carbon Cycling in Tropical Lowland Flooded Rice Ecosystem | Nutrient Cycling in Agroecosystems. Available online: https://link.springer.com/article/10.1007/s10705-013-9553-1 (accessed on 29 December 2023).

30. Chen, C.; Li, D.; Gao, Z.; Tang, J.; Guo, X.; Wang, L.; Wan, B. Seasonal and Interannual Variations of Carbon Exchange over a Rice-Wheat Rotation System on the North China Plain. *Adv. Atmos. Sci.* **2015**, *32*, 1365–1380. [CrossRef]

31. Liu, C.; Wu, Z.; Hu, Z.; Yin, N.; Islam, A.R.M.T.; Wei, Z. Characteristics and Influencing Factors of Carbon Fluxes in Winter Wheat Fields under Elevated CO_2 Concentration. *Environ. Pollut.* **2022**, *307*, 119480. [CrossRef]

32. Morales, D. Efecto de altas temperaturas en algunas variables del crecimiento y el intercambio gaseoso en plantas de tomate (*Lycopersicon esculentum* Mill. CV. AMALIA). *Cultiv. Trop.* **2006**, *27*, 45–48.

33. Li, C.; Li, Z.; Zhang, F.; Lu, Y.; Duan, C.; Xu, Y. Seasonal Dynamics of Carbon Dioxide and Water Fluxes in a Rice-Wheat Rotation System in the Yangtze-Huaihe Region of China. *Agric. Water Manag.* **2023**, *275*, 107992. [CrossRef]

34. Saito, M.; Miyata, A.; Nagai, H.; Yamada, T. Seasonal Variation of Carbon Dioxide Exchange in Rice Paddy Field in Japan. *Agric. For. Meteorol.* **2005**, *135*, 93–109. [CrossRef]

35. LI-7500|Support. Available online: https://www.licor.com/env/support/LI-7500/home.html (accessed on 2 January 2024).